Developing a Gas Nozzle for Laser Wakefield Acceleration

L. Concini [1], Dr. N. Beier[1], A. Ojonoka Yusuf[1], Dr. A. Hussein[1,2]

[1]Department of Electrical and Computer Engineering, University of Alberta, Edmonton, Canada
[2]Department of Physics, University of Alberta, Edmonton, Canada

Introduction

Motivation

Laser wakefield acceleration (LWFA) uses an ultrashort, high-intensity laser pulse interacting with a gas target to form a plasma structure and accelerate an electron beam to MeV or GeV energies. LWFA uses acceleration gradients 1000× stronger than those in traditional RF systems, reducing accelerator cost and size. LWFA requires precise laser-plasma characteristics. Each laser needs a tailored gas target to control acceleration parameters.

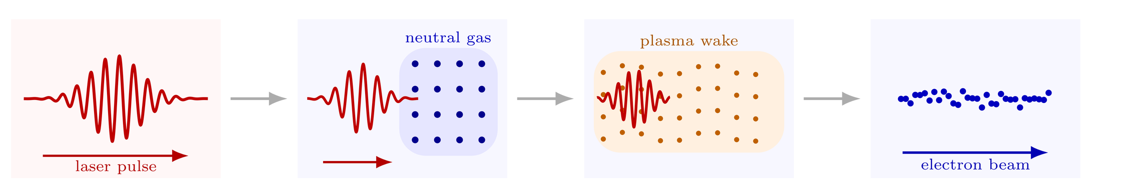

Objectives

This project designs and develops a gas nozzle for future LWFA experiments. We will:

1. Simulate nozzle geometries to measure plume parameters;
2. Build an optical setup to test the nozzle;
3. Validate the design and identify improvements.

Design

Scaling Laws

Laser wavelength λ and pulse energy E_{pulse} dictate required optical and plasma characteristics [1], [2]. We vary pulse length τ and normalized vector potential a_0 until resonance conditions converge. This sets the gas density via the required plasma electron density:

$$\underbrace{\omega_p \approx \frac{2\sqrt{a_0}\,c}{w_0}}_{\text{plasma frequency}} \rightarrow \underbrace{n_e = \frac{\epsilon_0 m_e \omega_p^2}{e^2}}_{\text{electron density}} \rightarrow \underbrace{He \rightarrow He^{2+} + 2e^-}_{\text{gas ionization}}.$$

Gradient lengths must not exceed the Rayleigh length to limit diffraction through phase objects:

$$L_{\text{grad}} < z_R = \frac{\pi w_0^2}{\lambda}.$$

We optimized for an 800 nm, 500 mJ terawatt laser system.

Ansys Fluent CFD Simulations

We used Ansys Fluent CFD simulations to optimize a de Laval nozzle for the desired density and spatial profile.

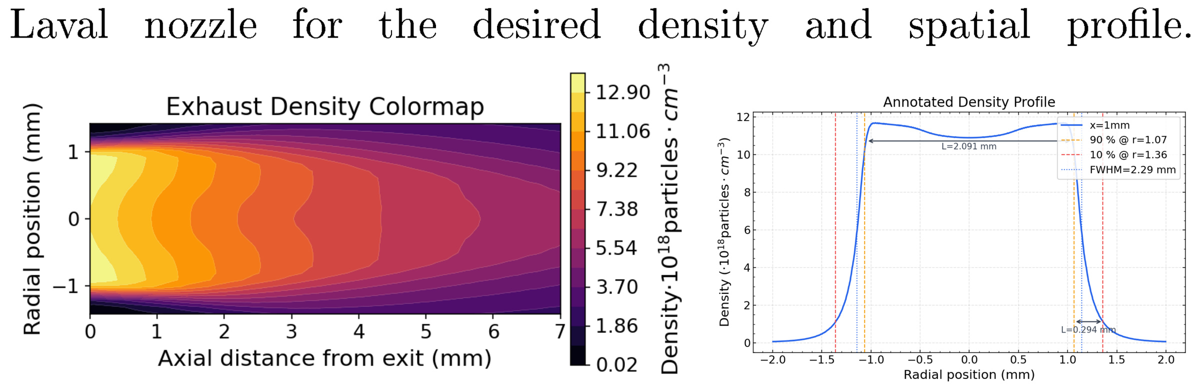

Figure 1: Simulated exhaust plume contours (left) and radial density lineout (right) for argon at 400PSI.

We quantify density gradient length from the profile *rise time*. Boundary layer thickness, slow-moving gas layers along nozzle walls, determines the density gradient sharpness. We will validate the nozzle prototype by comparing experimental results with simulations.

Methods

We optimized resin printing parameters and geometry to attain the maximal 50μm transverse resolution without warping and layer separation. The final prototype in Figure 2 is a de Laval structure with an O-ring sealing the gas inlet.

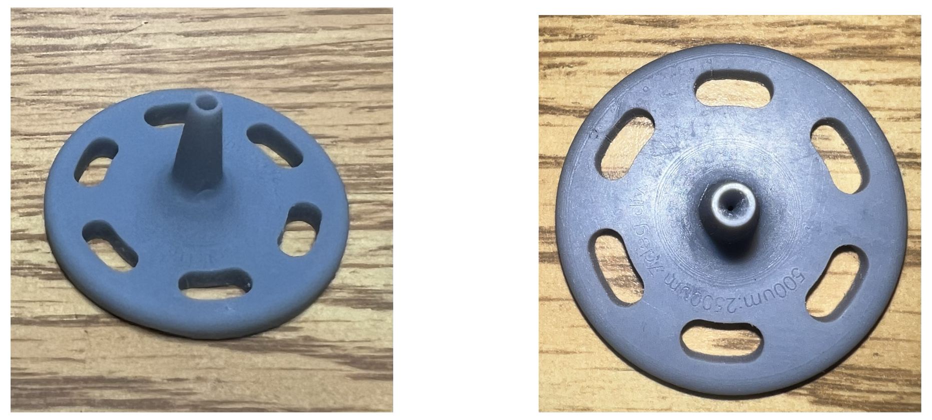

Figure 2: The final resin printed nozzle prototype.

For a given gas, the Gladstone-Dale relation links refractive index n to neutral-gas density ρ [3], [4]:

$$n = k\rho + 1 \quad (1)$$

A probe beam accrues phase ϕ while propagating through the gas [5]:

$$\phi(x, y) = \frac{2\pi}{\lambda}\int_L n(x, y, z, \lambda)\, dz = \frac{2\pi}{\lambda} L\overline{n}(x, y, \lambda) \quad (2)$$

A Mach-Zehnder interferometer measures phase shifts through interference between reference and probe beams at angle θ, creating alternating intensity fringes [6]:

$$I \propto 1 + \cos\left[2x\sin\left(\frac{\theta}{2}\right)\right] \quad (3)$$

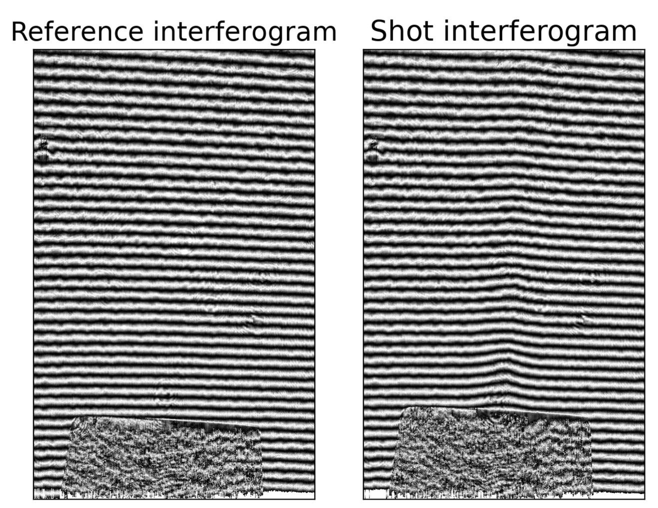

Figure 3: Bending of interference fringes at the nozzle exit during gas flow (right) compared to background (left) encodes density data.

We extract the gas density from the bending of fringes when the nozzle is activated under vacuum, as in Figure 3. We designed an optical experiment using a HeNe laser and Mach-Zehnder interferometer to image the fringes onto a CCD camera, seen in Figure 4 and Figure 5.

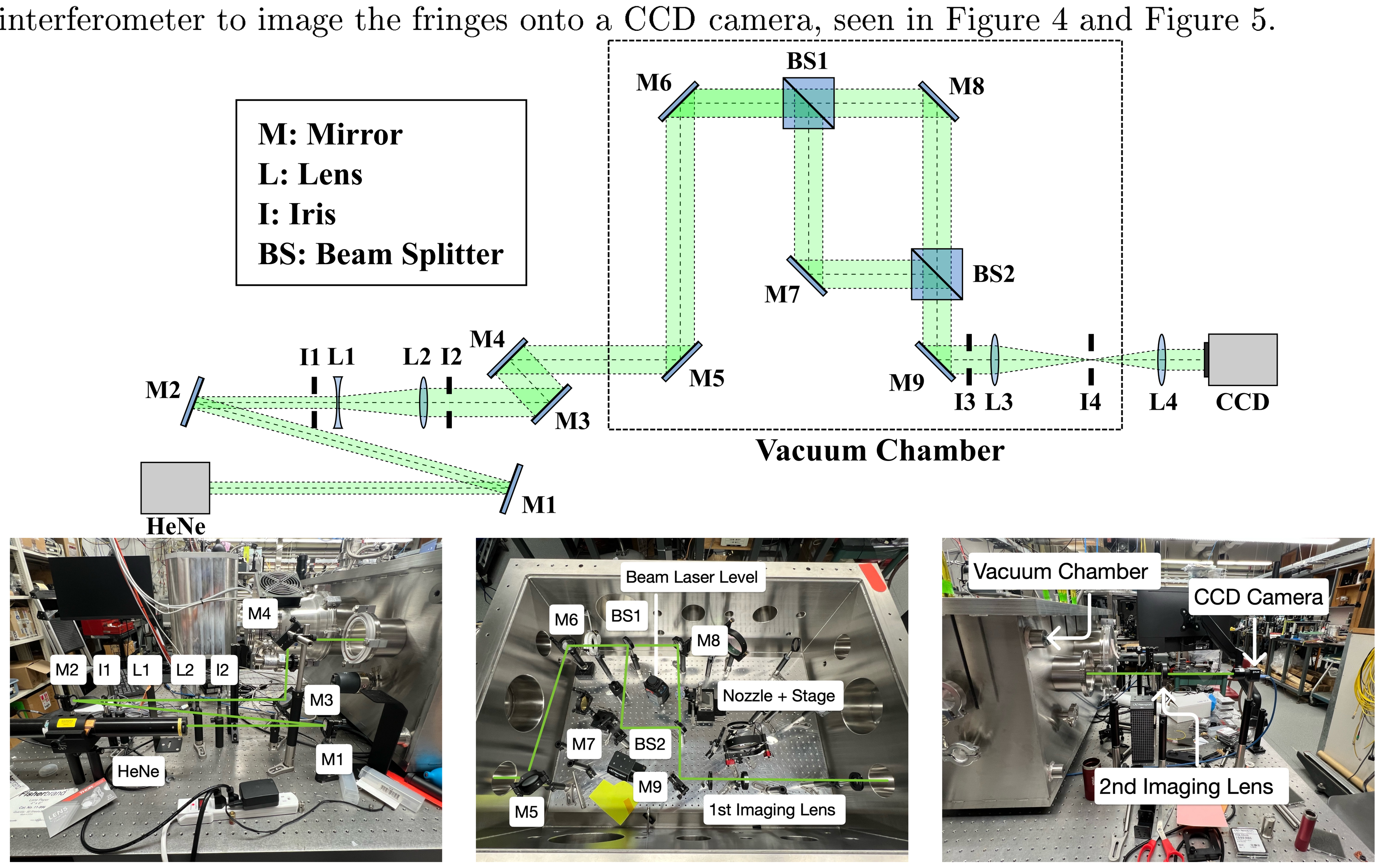

Figure 4: (top) A schematic of our optical setup for the neutral gas density Mach-Zehnder interferometry. (bottom, left to right) HeNe alignment stage; Mach-Zehnder interferometer; 4f imaging system.

Interferogram phase shift measures line-averaged plume density. Abel inversion recovers the radial density from the cylindrically symmetric plume.

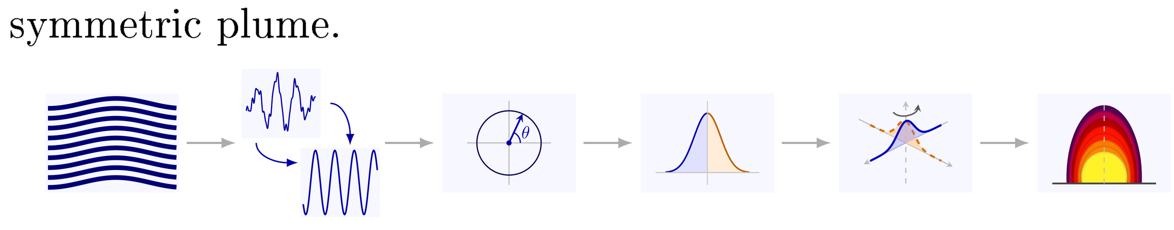

Interferograms were collected with argon at 400PSI into 100 Pa vacuum. Ansys Fluent simulations benchmark the results.

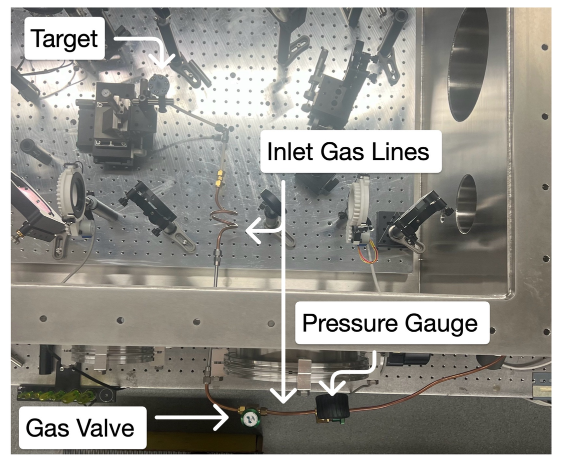

Figure 5: The gas lines for supplying argon into the de Laval nozzle.

Results

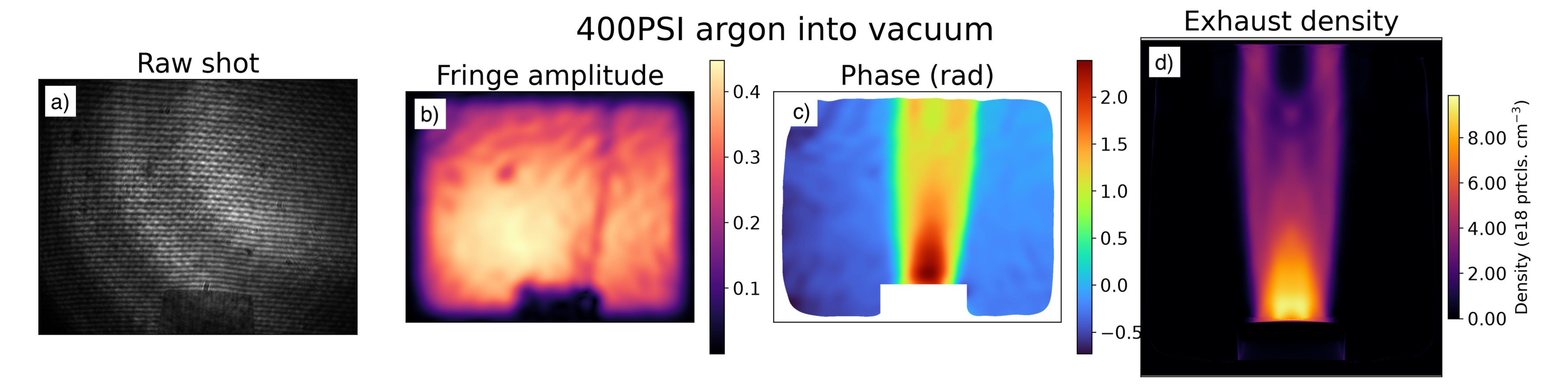

Figure 6: a) Raw interferogram; b) amplitude map; c) phase map; d) Abel-inverted density distribution.

Interferogram processing is shown in Figure 6. Experimental and simulated density distributions are compared in Figure 7 and Figure 8.

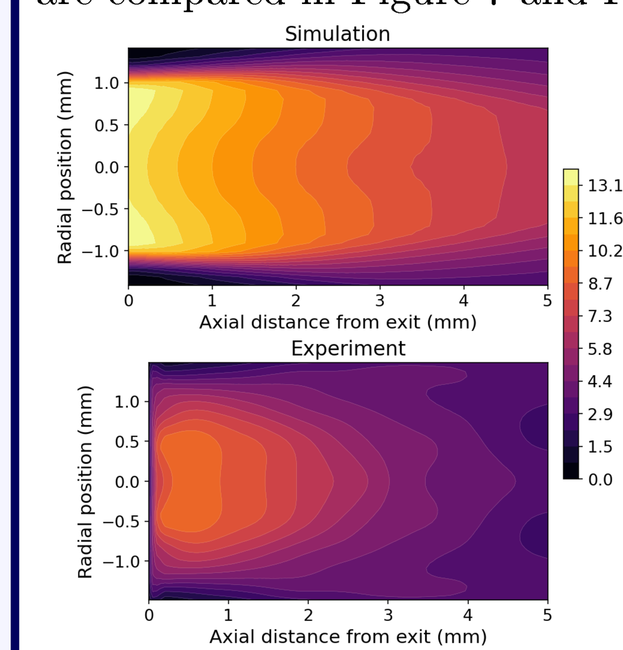

Figure 7: Comparison of simulated and experimental density contours.

Profiles generally match simulations but lack fine-scale agreement. Results:

- Conical exhaust plume in Figure 7 confirms supersonic flow;
- Experimental plume is diffuse, with large FWHM in Figure 8;
- Broad density gradients contribute to large FWHM;
- Broader plume yields peak experimental densities ~ 75% of simulation.

Primary error sources:

- Transverse resin printer resolution is 10% of the smallest geometry;
- Printed layer structure exacerbates boundary layers, causing diffuse gradients.

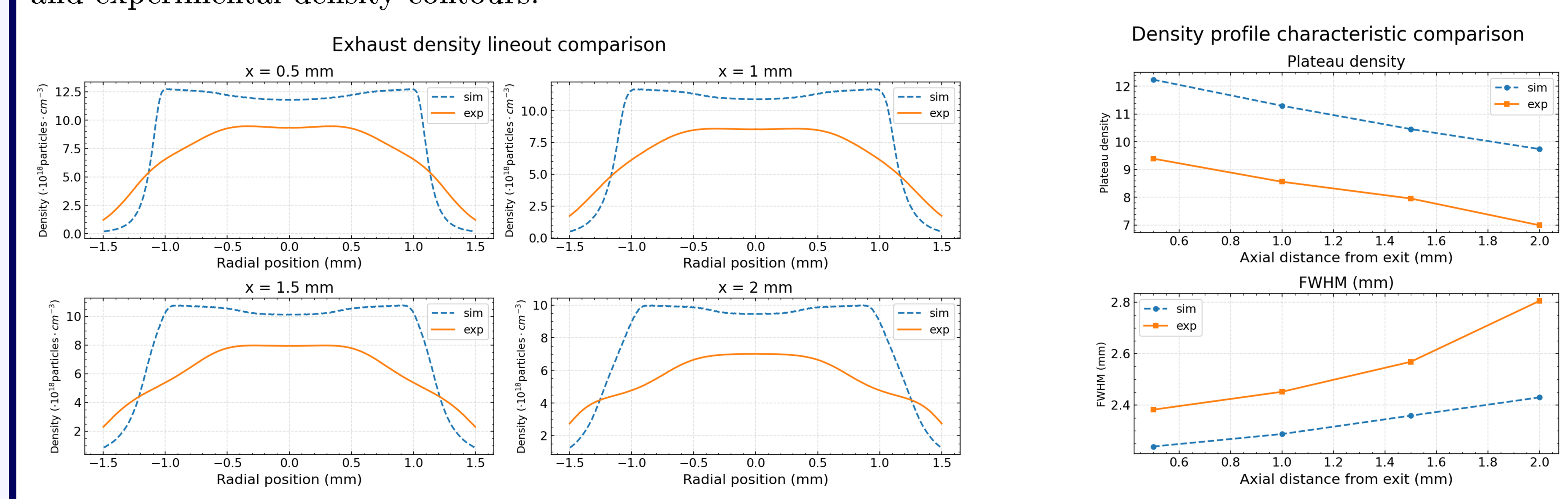

Figure 8: Comparison of simulated and experimental density lineouts at differing distances from the nozzle exit (left), and density profile metrics (right).

Conclusions

→ Nozzle produces a supersonic gas plume consistent with simulation;
→ Manufacturing precision limits experimental accuracy.

We demonstrate a viable LWFA nozzle design procedure; further refinement is necessary before use in experiment. Higher-precision manufacturing (e.g. micro spark erosion), would reduce gradient lengths and restore expected densities.

References & Acknowledgements

References

[1] J. Faure et al., "A review of recent progress on laser-plasma acceleration at khz repetition rate," *Plasma Physics and Controlled Fusion*, vol. 61, no. 1, p. 014012, 2019.

[2] W. Lu et al., "Generating multi-gev electron bunches using single stage laser wakefield acceleration in a 3d nonlinear regime," *Physical Review Special Topics—Accelerators and Beams*, vol. 10, no. 6, p. 061301, 2007.

[3] M. N. Polyanskiy, "Refractiveindex.info database of optical constants," in *Nature Scientific Data*, ser. Nature Scientific Data, vol. 11, Springer, Jan. 2024, 94, p. 94. DOI: 10.1038/s41597-023-02898-2

[4] NIST, *Experimental Polarizabilites (release 22)*, [Online]. Available: https://cccbdb.nist.gov/pollistx.asp, Gaithersburg, MD, 2022.

[5] F. Brandi and L. A. Gizzi, "Optical diagnostics for density measurement in high-quality laser-plasma electron accelerators," *High Power Laser Science and Engineering*, vol. 7, e26, 2019. DOI: 10.1017/hpl.2019.11

[6] J. M. Cole, "Diagnosis and application of laser wakefield accelerators," 2015. [Online]. Available: https://api.semanticscholar.org/CorpusID:114468308

Acknowledgements

I thank my supervisor, Dr. Amina Hussein, for the opportunity to work in her lab. I also thank Dr. Nicholas Beier and Abdulhakeem Ojonoka Yusuf for their invaluable mentorship and guidance. I am grateful for the support of the UAlberta Engineering Co-op Office and the Government of Canada NSERC/CRSNG USRA grant.